remote sensing

MDPI

Article

Non-Linear PSInSAR Analysis of Deformation Patterns in Islamabad/Rawalpindi Region: Unveiling Tectonics and Earthquake-Driven Changes

Zeeshan Afzal [1], Timo Balz [1,*] and Aamir Asghar [2]

[1] State Key Laboratory of Information Engineering in Surveying, Mapping and Remote Sensing, Wuhan University, Wuhan 430079, China; 2018276190014@whu.edu.cn
[2] Institute of Earth Sciences, University of Poonch, Rawalakot 12350, Pakistan; aamirasghar@upr.edu.pk
* Correspondence: balz@whu.edu.cn

Abstract: The standard Permanent Scatterer Interferometric Synthetic Aperture Radar (PSInSAR) technique, which is commonly used for surface motion analysis, assumes linear deformation velocities. While effective for monitoring urban subsidence over short periods, it falls short when dealing with non-linear, earthquake-related deformations over extended timeframes. To address this limitation, we use a non-linear PSInSAR technique, which is an enhancement of PSInSAR, to identify non-linear deformation patterns. We processed Sentinel-1A images from ascending and descending orbits in the Islamabad/Rawalpindi region from December 2015 to January 2023 using non-linear PSInSAR. By calculating the differences in deformation, we analyzed surface movements and assessed the impact of the 2017 earthquake on urban areas. Our findings reveal that the earthquake significantly increased the deformation in ascending and descending orbit tracks, with an average deformation of up to 70 mm/yr and a line-of-sight movement of up to 30 mm/yr. Our observations indicate that the deformation is directed towards the line of sight in the north and south of the deformed area, suggesting subsidence between the two uplifting faults, potentially linked to a concealed fault line along the deformation zone boundary. This contradicts previous arguments, suggesting that water extraction is the leading cause of deformation. Our analysis with non-linear PSInSAR demonstrates that tectonics play a significant role in deformation, providing valuable insights into tectonic-activity-induced deformations in urban areas over the long term.

Keywords: non-linear PSInSAR; deformation; earthquake-driven changes; tectonics

check for updates

Citation: Afzal, Z.; Balz, T.; Asghar, A. Non-Linear PSInSAR Analysis of Deformation Patterns in Islamabad/Rawalpindi Region: Unveiling Tectonics and Earthquake-Driven Changes. *Remote Sens.* **2024**, *16*, 1194. https://doi.org/10.3390/rs16071194

Academic Editor: João Catalão Fernandes

Received: 23 January 2024
Revised: 6 March 2024
Accepted: 13 March 2024
Published: 29 March 2024

Copyright: © 2024 by the authors. Licensee MDPI, Basel, Switzerland. This article is an open access article distributed under the terms and conditions of the Creative Commons Attribution (CC BY) license (https://creativecommons.org/licenses/by/4.0/).

1. Introduction

Many cities worldwide are situated in regions prone to instability. Various natural and anthropogenic factors can cause surface deformation in urban areas, including lithology [1,2], dewatering [3,4], tectonic activities [5], building loads [6], mining activities [7], and groundwater consumption [8]. These factors can individually influence the surface subsidence but often act in concert, amplifying the risk of hazards like building collapses, thereby posing a threat to the well-being of the urban population [9].

The Islamabad/Rawalpindi region, one of the most densely populated areas in Pakistan, lies in a seismically active zone. This area has experienced several major earthquakes, with a recent significant event in 2017. It is prone not only to frequent and severe earthquakes but also to land subsidence driven by groundwater withdrawal, urban development pressures, mining, and specific soil characteristics [10,11]. Monitoring surface deformation here is crucial for understanding tectonic activity and assessing seismic hazards. However, conventional methods for deformation monitoring, such as GPS and leveling, are limited by spatial coverage and cost, necessitating an alternative method that can provide high-resolution and long-term deformation measurements. In light of these challenges,

Permanent Scatterer Interferometry (PSInSAR) is a promising solution for monitoring and detecting surface deformations in densely populated regions.

Background

PSInSAR is a powerful tool for monitoring surface deformation with high accuracy and precision over large areas by analyzing the phase differences between multiple Synthetic Aperture Radar (SAR) images. Its versatility is evident in its widespread applications in geoscience fields, such as volcanology, seismology, hydrogeology, and geotechnical engineering [12]. It plays a pivotal role in detecting and measuring deformations associated with seismic events, contributing significantly to earthquake research [13]. It aids in studying the impact of urbanization on groundwater stress and land deformation [14]. Its utility extends to assessing the structural stability and safety of artificial structures including dams [15], bridges [16], tunnels [17], and buildings [18].

The core strength of PSInSAR lies in the utilization of Permanent Scatterers (PSs)—coherent radar targets whose stability over time ensures accurate displacement measurements [19]. This technique addresses several limitations of conventional differential InSAR (DInSAR), such as atmospheric artifacts, temporal decorrelation, and spatial baseline constraints [12]. Recent advancements in PSInSAR technology, including algorithms like StaMPS (Stanford Method for Permanent Scatterers) [20], SBAS (Small Baseline Subset) [21], and SqueeSAR [22], have further enhanced its capability to identify a higher density of valid PS points and reduce atmospheric and orbital effects, thereby improving accuracy in densely populated urban areas.

However, despite these advancements, conventional PSInSAR techniques typically assume linear deformation over time, which can be insufficient for accurately capturing the complexities of long-term and non-linear deformation processes [23]. This limitation was highlighted in a case study of surface deformation in Islamabad and Rawalpindi, where PSInSAR initially pinpointed water extraction as the main factor, neglecting the region's tectonic movements [24]. Despite the detection of a magnitude 4.6 earthquake in 2017, indicative of tectonic activity, a short-term study from January 2019 to June 2021 failed to capture the earthquake's impact or fully evaluate tectonic influences.

Addressing this gap, our study introduces the non-linear PSInSAR technique for comprehensive long-term linear and non-linear urban deformation monitoring. By applying non-linear PSInSAR analysis from 2015–2023, we captured subtle, earthquake-linked velocity variations in Islamabad–Rawalpindi that linear PSInSAR would overlook. Independent velocity estimation over sequential windows allowed us to detect these variations, revealing significant tectonic influences on observed surface changes. Our study indicates that tectonic activities significantly influence the observed surface changes, challenging prevailing assumptions that anthropogenic factors drive deformation. We further employed the vertical displacement decomposition (VDD) method [25] on ascending and descending datasets, which enabled us to determine the vertical displacement and quantify the deformation patterns over time.

2. Study Area

The twin cities of Islamabad and Rawalpindi lie to the east of the North Potwar deformed zone (NPDZ), which is a tectonically active zone and part of the Salt Range and Potwar Plateau (SR/PP) [26] and geologically part of the Sub-Himalayas [27]. Earlier, the NPDZ was examined by combining seismic, borehole, and paleomagnetic data, as well as surface geology, to understand the complex structures and development stages [28,29]. The eastern NPDZ has a geological history of approximately 150 Myr from the Middle Jurassic to the Quaternary, and the oldest rocks in the study area are Jurassic marine limestone and dolomites. The source of the deformation in the Eastern NPDZ is the basement fault and thinning of the evaporate facies [30]. Complex structures have been formed due to convergence, which causes high deformation, and the interpretations say that during the

evolution of the NPDZ, multiple back thrusts in the area caused uplifting and erosion several times [31].

Figure 1 shows a map of the study area, showing several passing faults. This map shows many tectonic features surrounding the study area. We observed the main boundary thrust (MBT), Golra thrust (GT), Bokra thrust (BT), Khairi Murat thrust (KMT), Dhurnal back thrust (DBT), Soan syncline, Riwat thrust (RT), and blind faults between BT and KMT in the study area.

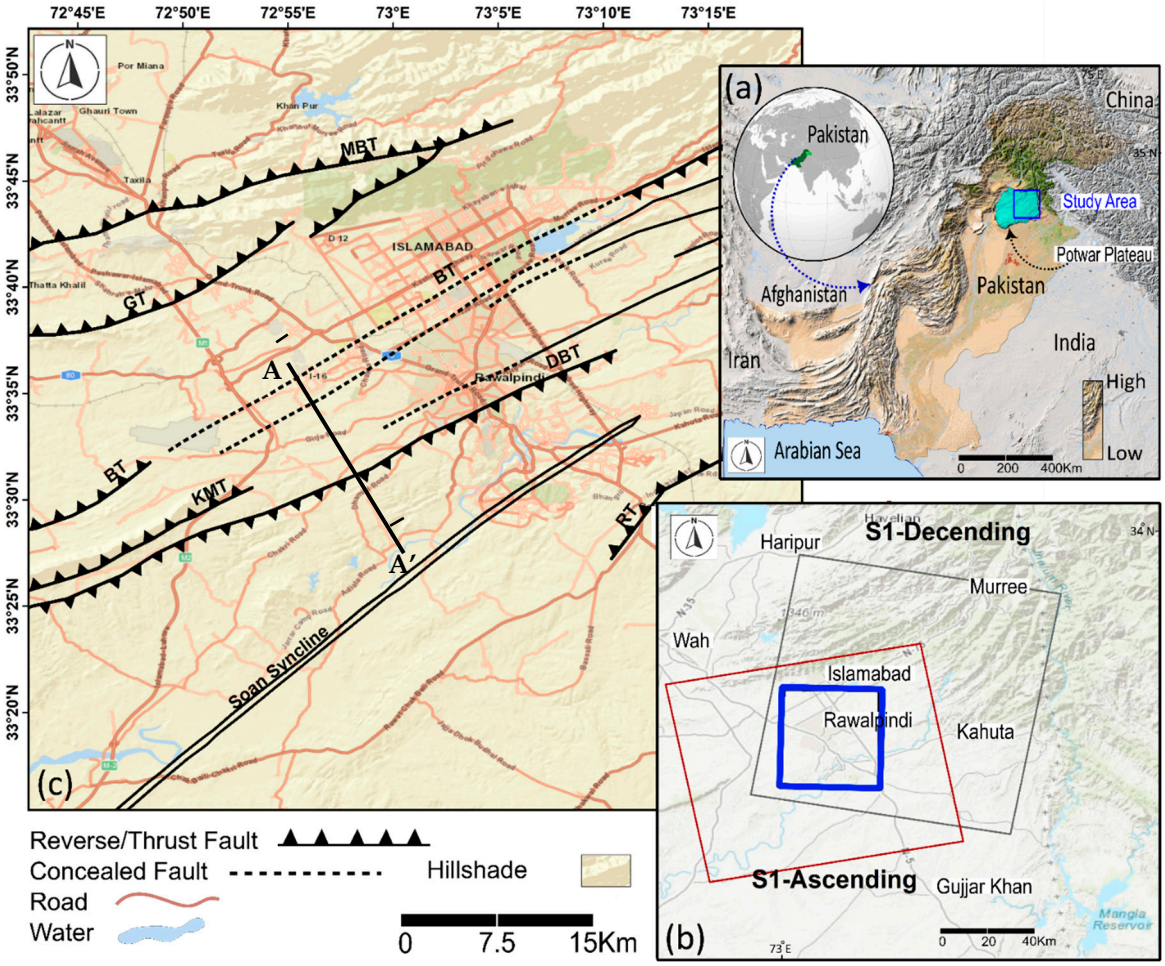

Figure 1. Study area map illustrating the delineation of faults and the coverage of Sentinel-1 imagery over the seismically active Potwar Plateau, focusing on the Islamabad and Rawalpindi cities: (**a**) the dark blue polygon shows the study area under consideration (topographic map provided by ArcGIS) located in the east of the NPDZ; (**b**) the grey polygon indicates the descending footprint, and the red polygon shows the ascending footprint of Sentinel-1 IW SLC images used for this study; (**c**) the structural classification of faults (modified from [32]), where AA′ shows the location of the cross-section discussed in the results.

The significance of tectonics in the study area is illustrated in Figure 1, which shows that the study area is surrounded by numerous structural faults, including thrust, reverse, and concealed faults. We used ascending and descending orbit track Sentinel-1 satellite images to monitor the study area, as shown in Figure 1b. The dark blue polygon represents the master area or common area, whereas the ascending and descending areas are denoted by red and light black polygons, respectively. To further understand the tectonic movement within the study area, the AA′ profile is drawn to show the cross-section in the results.

The study area was also affected by earthquakes within 10 km. Table 1 lists the number of events that occurred along different fault types, most of which occurred along concealed or blind faults. The activation of the NPDZ has been documented in historical records dating back to 1875, during which seismic events within the range of 4.6 to 6.7 M_w have been recorded. In 2017, a seismic event of magnitude 4.6 M_w occurred along the KMT. Although no discernible loss was inflicted on nearby infrastructure, this indicates that the region is tectonically active and has the potential to generate seismic hazards.

Table 1. Earthquakes >4 M_w in 10 km of our study area were obtained from the International Seismological Centre (2018) ISC-GEM Earthquake Catalogue [33]. M_w is the earthquake magnitude, whereas the fault type shows the fault that was the source of the earthquake.

Serial No.	Lat	Long	M_w	Year	Fault Type
1	33.57	72.99	4.6	2017	Concealed/Blind
2	33.60	72.90	5.3	1988	Concealed
3	33.50	73.10	5.2	1986	Normal
4	33.68	73.12	4.6	1977	Concealed/Blind
5	33.69	73.13	4.1	1977	Concealed/Blind
6	33.69	73.14	4.0	1977	Concealed/Blind
7	33.62	73.07	6.7	1869	Concealed/Blind
8	33.49	73.01	6.0	1875	Thrust

Table 1 lists the locations of the earthquakes within specific years and magnitudes. From Table 1, we observe that seismic activity has caused this area to be unstable, and the primary source of the earthquakes is concealed/blind faults, which have affected the study area more than six times in the past. Several studies have been conducted to understand the geology of this study area.

Regionally, the MBT in the north and the Soan syncline in the south are the main tectonic structures, as shown in Figure 1, and 55 km of shortening between 8 and 5 Myr was observed between them [31]. The MBT stretches from the Afghan border and is traced to Assam in eastern India to a close distance in the north of the NPDZ and represents the major zone of recent deformation and the largest earthquakes in the world [34]. The Soan syncline is the main geological feature of the SR/PP. It separates highly complex and deformed Lower to Middle Miocene Rawalpindi group strata in the north by about 20 km from the less deformed Upper Miocene to Pliocene Siwalik strata in the south [35]. Repetition in these strata was observed in the Rawalpindi group, and many faults were concealed by alluvial deposits [36].

Towards the north, other than the main boundary thrust (MBT), the Golra thrust (GT) and Bokra thrust (BT) are the major thrust faults, and geological features, including topography, fault breccia, and seepage of water in specific locations, provide information about the faults in the area. More than 3 km thick Middle Miocene to Quaternary Siwalik strata disappeared in the north of the Soan syncline, and the Soan back thrust, also named Dhurnal back thrust, and the Khairi Murat thrust both are the major fault lines [37] in the south of the Eastern North Potwar deformed zone (NPDZ). Therefore, this study holds particular relevance in a densely populated region encompassing the twin cities, where the population exceeds 4 million [38], allowing us to gain insights into the deformation patterns and the seismic impact within this tectonically active area.

3. Materials and Methods

In this section, we present the methodology for applying the non-linear PSInSAR technique to the study area of Islamabad/Rawalpindi and its surrounding area. We aim to detect and analyze surface motion over a long period using Sentinel-1 SAR images.

3.1. Datasets

For our study, we utilized a dataset consisting of 349 Sentinel-1 C-band single-look complex scenes for both ascending (189 images) and descending (160 images) geometries to conduct a wide-area analysis of the twin cities (Islamabad/Rawalpindi) and their surrounding areas. Sentinel-1 C-band SAR images are ideal for our study because they are freely available from the Copernicus Data Space Ecosystem (https://dataspace.copernicus.eu/, accessed on 3 February 2023).

Furthermore, Sentinel-1 single-look complex (SLC) images have a spatial resolution of 5 m × 20 m in interferometric wide swath mode, which allows the detection of small-scale deformation features. Additionally, Sentinel-1A has a revisit time of 12 days, which enables us to capture the temporal evolution of surface motion and reduce temporal decorrelation.

During the analysis of the study area, both ascending and descending tracks of Sentinel-1 images were processed using the non-linear Permanent Scatterer Interferometry (PSInSAR) tool in the SARPROZ software package [39]. Subsequently, deformation maps were generated from these tracks which were superimposed on Google Earth and a tectonic map to visually represent deformation patterns in the study area.

3.2. Non-Linear PSInSAR Processing

The methodology employed in our study represents a departure from the conventional linear motion assumptions typically utilized in surface motion analysis. The traditional assumption of linear deformation velocity in the PSInSAR technique has proven to be effective for urban subsidence studies within constrained timeframes. However, when investigating the surface motion caused by tectonic activities over more extensive durations, relying solely on linear models is not valid. Recognizing the limitations inherent in the linear models, especially in the context of long-term tectonic deformation studies, our study adopts a non-linear PSInSAR approach.

The proposed non-linear PSInSAR approach involves the independent estimation of velocity over time. Unlike the traditional PSInSAR approach, which seeks to minimize the residual phase by estimating the height change (Δh) and linear motion velocity ($\Delta vlinear$) concurrently, the non-linear methodology employs a segmented approach. This facilitates a more granular analysis of deformation over shorter intervals, enhancing the understanding of the intricate dynamics at play.

In the non-linear estimation of point pairs, we first estimate a height value h, which is assumed as a constant over all acquisitions. The model leverages the principle of coherence maximization across the interferograms, expressed as follows:

$$\hat{h} = \underset{\hat{h}}{\arg max} \left\{ \frac{1}{N-1} \sum_{i=1}^{N-1} \left| exp(-i(\phi_i - \phi_{i,h})) \right| \right\} = \underset{\hat{h}}{\arg max} \left\{ \frac{1}{N-1} \sum_{i=1}^{N-1} \left| \exp\left(-i\left(\phi_i - \frac{4\pi B_{p,i} \hat{h}}{\lambda R_i \sin \alpha_i} \right) \right) \right| \right\} \quad (1)$$

where λ is the wavelength, R is the range distance, α is the incidence angle, and B_p is the perpendicular baseline. The velocity of every n_s consecutive interferogram is estimated as follows:

$$\hat{v} = \underset{\hat{v}}{\arg max} \left\{ \frac{1}{n_s - 1} \sum_{i=1}^{n_s} \left| \exp\left(-i\left(\phi_i - \phi_{i,h} - \frac{4\pi \hat{v} t_i}{\lambda} \right) \right) \right| \right\} \quad (2)$$

where t is the temporal baseline. The estimation of v is performed like a moving window along N SAR images. By integrating the instantaneous v of every scene, the individual deformation of each scene can be obtained.

In the non-linear PSInSAR methodology, we approach velocity estimation through a more targeted window of interferograms rather than utilizing the entire dataset as done in conventional PSInSAR techniques. This involves selecting a specific set of 11 consecutive interferograms, encompassing 5 images before, 1 on, and 5 following the date of interest. This targeted selection is crucial for capturing the non-linear deformation patterns, which are often masked by the dominance of linear trends in larger datasets. However, it is

important to note that the exact number of interferograms (11, 15, 19, etc.) can vary based on the specific deformation patterns being analyzed.

By confining our analysis to this subset of interferograms, we enhance our ability to detect and understand non-linear deformation patterns that might be less apparent in a broader analysis. Furthermore, after estimating the velocity for each window, we proceeded to calculate the cumulative displacement for each Permanent Scatterer (PS). This step is crucial as it provides a more comprehensive understanding of the overall deformation in the study area.

3.3. Vertical Displacement Decomposition

After obtaining the line-of-sight (LOS) cumulative displacement of the ascending and descending geometries, the surface deformation in the entire study area was analyzed to create a continuous surface deformation for vertical displacement decomposition (VDD) processing. For the vertical displacement decomposition, we first merge all the PS points, and then we further obtain VDD using the matrix presented in Equations (3) and (4) [8,28]:

$$\begin{pmatrix} d_{asc} \\ d_{desc} \end{pmatrix} = A \begin{pmatrix} d_{vert} \\ d_{horiz} \end{pmatrix} \tag{3}$$

$$A = \begin{pmatrix} cos\theta_{asc} & \frac{sin\theta_{asc}}{cos\theta_{\Delta a}} \\ cos\theta_{desc} & sin\theta_{desc} \end{pmatrix} \tag{4}$$

In this equation, d represents the deformation along the line of sight (LOS) for the ascending deformation d_{asc} and descending d_{desc} modes. The term d_{vert} represents the vertical motion. The term d_{horiz} refers to the projection of horizontal deformation in a descending azimuth-look direction. θ is the incident angle, and $\Delta\alpha$ represents the satellite heading difference between the ascending and descending orbits. The estimated horizontal motion described in this matrix is mostly in the east–west direction. Owing to the near-polar orbit of Sentinel-1 sensors, the north–south horizontal motion is considered negligible, making accurate estimation challenging [40]. We also analyzed time series deformation data to observe yearly changes in the study area.

3.4. Yearly Time Series Change Analysis

To assess the impact of the 2017 earthquake on the study area, the time series deformation values of each PS (Permanent Scatterer) point were calculated and filtered, and the deformation values were separated for each year. By subtracting the initial deformation value from the final value for each year, specifically between 2016 and 2022 for the ascending dataset and 2017 and 2022 for the descending dataset, we examined the cumulative displacement over time. This approach allowed us to thoroughly analyze the impact of the earthquake from both ascending and descending tracks, enabling us to determine whether the observed effects were consistent across both directions. Furthermore, cumulative displacement values were analyzed to detect spatiotemporal deformation patterns across the study area.

By employing this methodology, we successfully captured deformation resulting from tectonic activity or abrupt changes that could have been easily missed using other techniques. This approach proved especially valuable for our comprehensive, long-term investigation, as it provided a means to quantify and analyze the overall non-linear motion. Moreover, it allowed us to gain new insights into the impact of the earthquake on the deformation zone, revealing previously unobserved phenomena [24].

4. Results and Analysis

Expanding upon a previous PSInSAR study [24] that limited its scope to linear trends from January 2019 to June 2021, our comprehensive analysis introduces non-linear PSInSAR techniques, examining both linear and non-linear deformation trends over an extended seven-year period. The cumulative deformation map highlights significant subsidence and

uplift in various parts of both cities, particularly along their boundary, indicating a complex interplay between human activities and tectonic forces. This suggests that the causes of deformation in the study area are multifaceted, with both human activity and tectonic movements playing crucial roles. Post-2017 earthquake observations reveal an escalation in deformation within the zone, with predominant vertical subsidence, challenging prior assumptions of deformation causes. We estimated the average displacement per year for ascending and descending observations, as depicted in Figure 2, to elucidate the subsidence and uplift patterns, reinforcing the influence of tectonic activity.

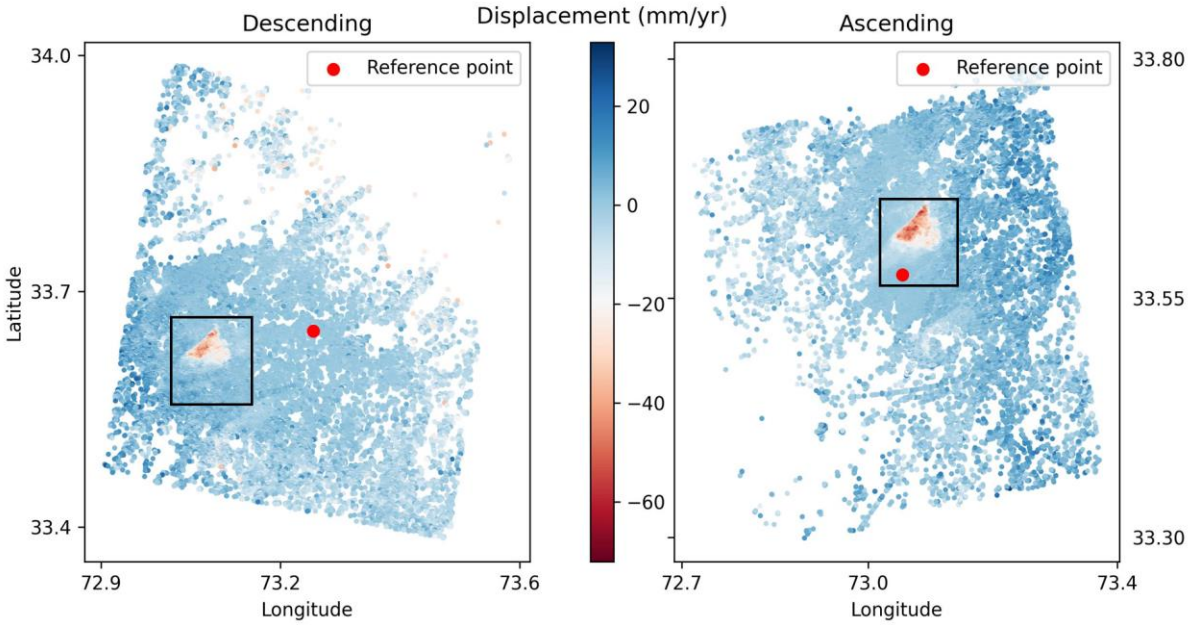

Figure 2. PS points distribution and displacement variation scatter plot of the study area from Sentinel-1A ascending (6 December 2015, to 22 January 2023) and descending (31 March 2017, to 23 January 2023) path, analyzed by non-linear PSInSAR, with deformation zone highlighted by the black polygon. The reference points for both descending and ascending motion are also shown as red points.

The non-linear PSInSAR analysis, applied to Sentinel-1A SAR data across both ascending and descending tracks, reveals a range of deformation rates, from −70 mm/year to +30 mm/year, as illustrated in Figure 2.

This analysis shows that while some areas exhibit stability or minor uplift, others, particularly within a designated black polygon, experience pronounced deformation. The deformation patterns obtained from the ascending and descending tracks of Sentinel-1A SAR data differ within the deformation zone, and these differences become more pronounced towards the southwest of the deformation zone (depicted by light red in the ascending track), indicating horizontal movement, possibly stemming from a thrust fault. To better understand the subsidence patterns surrounding the deformation zone, we overlaid the subsidence data (Figure 2) on Google Earth imagery.

In our detailed analysis, ten Permanent Scatterers (PSs) were selected from the results obtained using the non-linear PSInSAR method along the deformation zone, considering ascending and descending paths. A time series analysis was conducted for each of these points of 1 to 5 in ascending and 6 to 10 in descending, on the right side of Figure 3, where they are labeled as PS1 to PS10. On the right side of the figure, PS1 depicts the time series displacement of point 1, which corresponds to the left side of the ascending path. Similarly, PS2 represents the time series displacement for point 2 and the remaining points. This analysis provides a deeper understanding of the causes of the deformation in the study area.

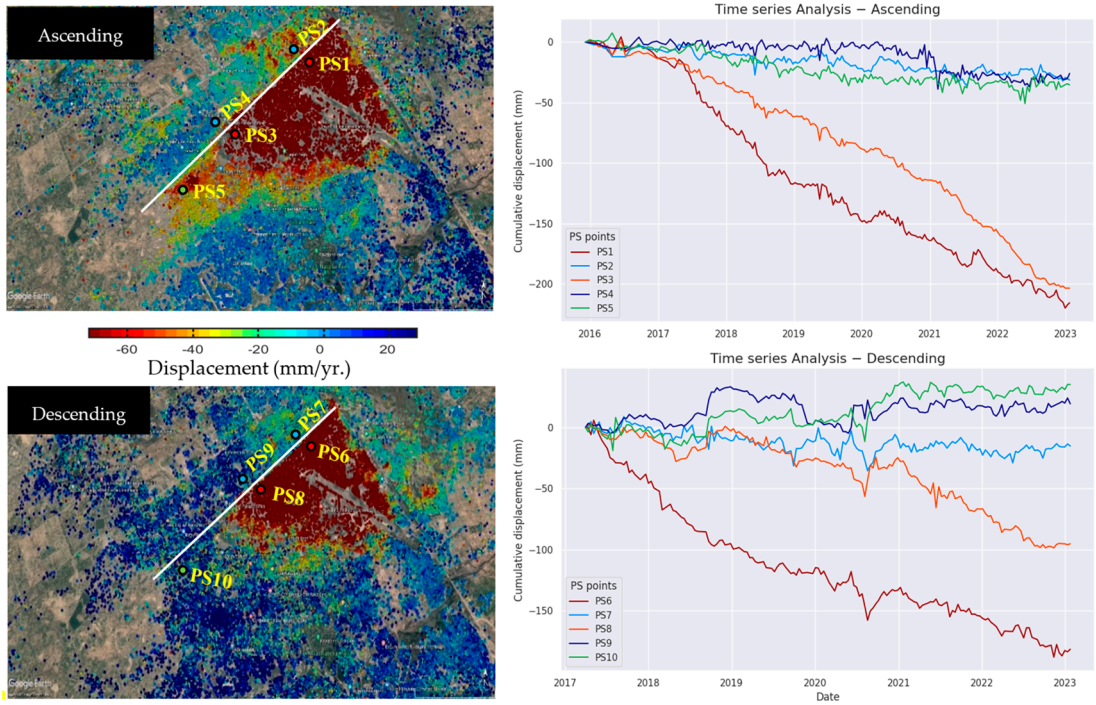

Figure 3. The deformation zone observed in Figure 2 in the black polygon displayed in Google Earth along with time series displacement of 10 PSs from both Sentinel-1A ascending (6 December 2015 to 22 January 2023) path and descending path (31 March 2017 to 23 January 2023) utilizing non-linear PSInSAR. On the left side, the deformation zone obtained by using non-linear PSInSAR from ascending and descending on Google Earth is displayed, while on the right side, the time series cumulative displacement of 1 to 5 in the ascending track and 6 to 10 in the descending track represented by PS1 to PS10 is displayed. The dark blue and sky blue colors represent the time series for PS away towards the north side of the white line. In contrast, the dark red and orange-red colors represent the deformation of the PS points south of the white line, whereas the time series displacement of PS5 and PS10 in the southwest is shown in green.

The presence of tectonic features in the study area is indicated by the abrupt change in deformation along the white line observed in both orbit tracks, as shown in Figure 3.

Upon analyzing the individual points along the ascending track, it became evident that there were considerable decreases in the displacement values. PS1 (−215 mm), located in the south, represented the time series of PS1, while PS2 (−31 mm), situated in the north, represents 2. Despite the relatively short distance between these two points, the difference in displacement values was significant. Similarly, notable differences were observed between the displacement values of PS3 (−203 mm) and PS4 (−26 mm). Such disparities underscore the pronounced variation in deformation along the critical zone, vividly captured in Figures 2 and 3. The significant variation in displacement values across short distances, as evidenced between PS1 and PS2, and PS3 and PS4, highlights the spatial variability of deformation within the critical zone.

Furthermore, the descending track analysis indicates a noticeable decrease in deformation values, suggesting a downward trend in the area's deformation pattern. This pattern aligns with observations made from ascending track data. We observed distinct deformation values for PS6 (−181 mm) and PS8 (−95 mm), while in the north, nearby points such as PS7 (−15 mm) and PS9 (−5 mm) exhibited very similar deformation values but with a declining trend.

Moreover, Figure 3 shows significant variations in the deformation trend between the ascending and descending directions, particularly towards the southwest. These variations suggest the possibility of horizontal movement in the study area, potentially caused by the thrust faults. A gradual decrease in deformation values was observed towards the

southwest in PS5 (−35 mm) from the ascending track. The sudden change along the straight deformation feature is evident from the ascending track, prompting us to analyze it from the descending track and determine if the changes are consistent. However, in contrast to the ascending track data, we observed an opposite pattern in the values for PS10 (35 mm) from the descending track. These points exhibited movement towards the line of sight (LOS).

Figure 3 reveals a sharp and clear shift in deformation values along the delineated white line, spotlighting a critical boundary of change. The PS points on the northern side of the line exhibited significantly lower deformation values than those on the southern side of the deformation zone. This discrepancy challenges the view that human activity, specifically water extraction, was the only cause of deformation in the area, and it indicates that alternative factors were in play. Furthermore, significant variation was observed between the ascending and descending tracks, particularly towards the southwest of the deformation zone. While the descending track displays movement towards the LOS, the ascending orbit track demonstrates movement away from the LOS, suggesting horizontal movement within the study area. These findings indicate the presence of a thrust fault, supported by recent earthquake activity along the fault line in the southwest of the deformation zone.

4.1. Effect of an Earthquake in the Study Area

Exploring the temporal evolution of deformation due to the 2017 earthquake near the deformation zone, we crafted yearly deformation maps for both ascending and descending tracks. The ascending track data from 2016 to the present revealed a persistent subsidence trend within the city, illustrating the spatial distribution of deformation and its changes over time (Figure 4). This analysis provides deeper insights into the earthquake's impact on deformation, highlighting variations across different areas.

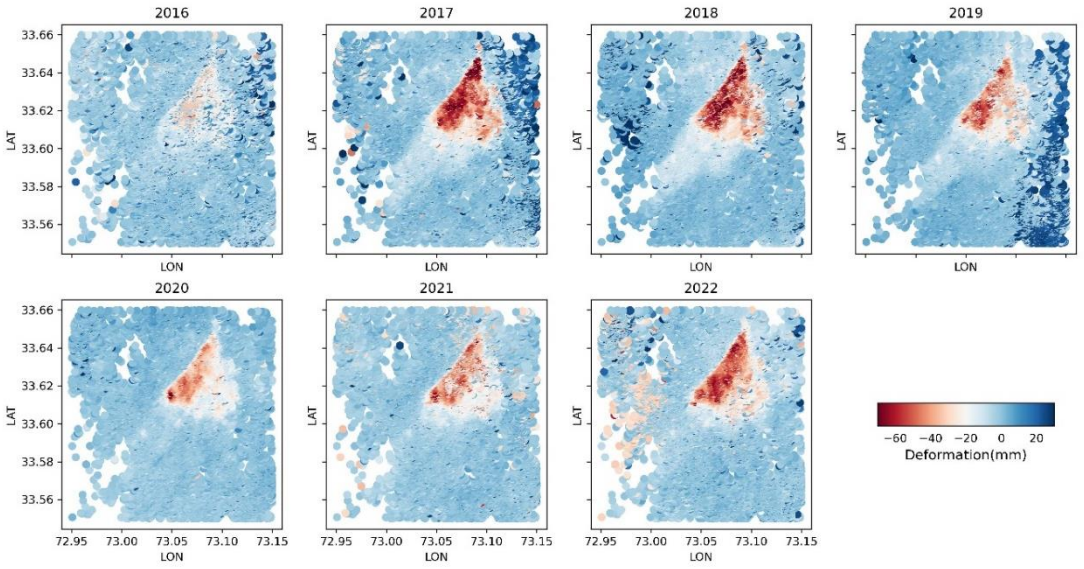

Figure 4. Non-linear PSInSAR time series analysis of the deformation zone by Sentinel-1A ascending track from 2016 to 2022.

The 2017 seismic event significantly impacted the deformation zone within the study area, as shown in Figure 4. The figure not only indicates pre-existing deformation in the study area before the earthquake, possibly due to water extraction or tectonic movement, but also a marked surge in deformation in 2017 and 2018. This underscores the critical role of tectonic forces, challenging earlier interpretations that predominantly focused on anthropogenic factors.

Analyzing the deformation patterns before and after the 2017 earthquake, as depicted in Figure 4, we observed a notable increase in subsidence in the twin cities from 2016 to 2017. This increase is visually represented by a distinct change in color on the deformation

map, signifying the earthquake's tangible impact. Moreover, while deformation in the study area remained relatively consistent from 2018 to 2019, an unexpected rise in subsidence was detected in 2022—despite the absence of reported tectonic activity. The reasons for this deformation pattern remain unclear, necessitating further investigation to better understand the underlying causes. It is worth mentioning that deformation caused by tectonics may exhibit varying directions along the line of sight from one orbital track to another, particularly if the deformation source is a thrust fault.

In response to the 2017 earthquake, the impact on deformation patterns is also evident in the descending track analysis using non-linear PSInSAR, as shown in the generated deformation maps (Figure 5). Although limitations exist, such as the exclusion of data from 2016 to 31 March 2017, due to the unavailability of descending track data, the subsequent years offer valuable information about the changing deformation patterns, indicating the lasting influence of the 2017 earthquake.

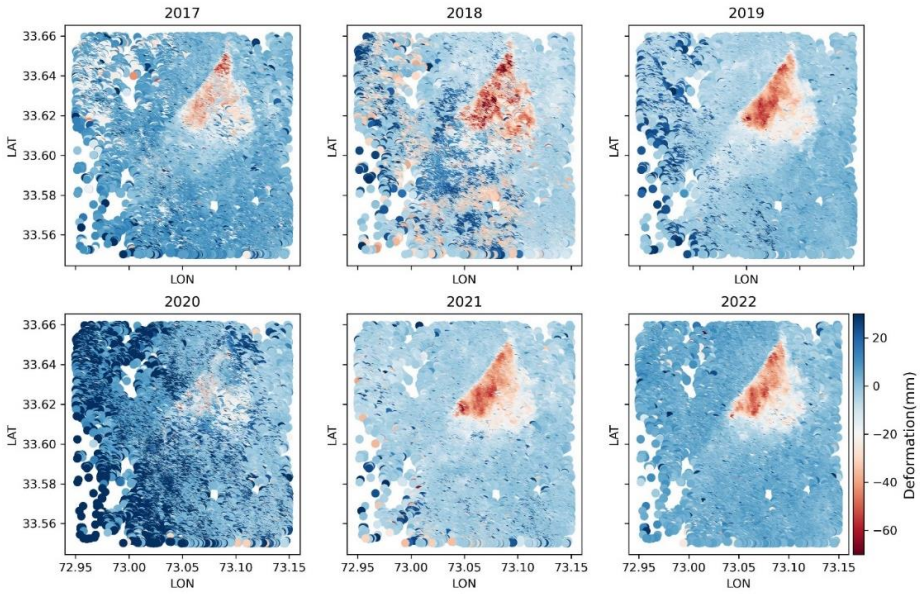

Figure 5. Non-linear PSInSAR-based time series deformation analysis of the deformation zone shown in Figure 3, as observed by Sentinel-1A descending track from 2017 to 2022.

The analysis of the descending track in Figure 5 reveals a substantial increase in deformation towards the northeast in 2018 compared to 2019, providing clear evidence of the 2017 earthquake's influence on the deformation zone. Furthermore, a distinct movement towards the line of sight (LOS) is observed in the southwest, in contrast to the movement away from LOS in the ascending track data, suggesting the presence of a thrust fault in the study area. This evidence disrupts the previous understanding that water extraction alone drives the area's deformation, pointing instead to a more complex interplay of factors.

The deformation analysis is subject to limitations owing to the unavailability of descending track data until March 2017, resulting in a lack of a four-month analysis for that year. As a result, Figure 5 does not capture the earthquake's immediate impact in 2017, leaving a gap in the visual record. Nevertheless, from 2018 onwards, a notable increase in deformation is observed, setting it apart from previous and subsequent years. This increase is depicted in Figure 5, where an intense red color indicates a substantial deformation. Concurrently, a noticeable movement towards the LOS in the southwest region indicates thrust fault movement in the study area.

In 2019, a distinct trend emerged with observable movement away from the LOS within the study area, contrasting with the patterns from the previous year. The deformation analysis for 2020 exhibits a unique pattern compared to previous years, characterized by minimal movement away from the LOS and a more pronounced movement towards the LOS, suggesting anomalous behavior.

Across 2021 and 2022, a consistent deformation pattern emerges in the descending track, aligning with the ascending data's observed trend. This pattern demonstrates a consistent subsidence alignment with the trends observed in the ascending track data. We employed a decomposition technique for ascending and descending orbit geometries to determine the vertical displacement.

4.2. Vertical Displacement

A more comprehensive understanding of vertical displacement can be obtained by examining the vertical displacement map, as shown in Figure 6. This map presents the vertical displacement decomposed from both the ascending and descending line-of-sight (LOS) geometries. In the map, areas exhibiting negative values, represented by the red to light yellow color range, signify subsidence, indicative of the ground surface's downward movement. Conversely, areas with positive values, shown in blue, suggest stability or a slight uplift, indicating an upward ground surface trend.

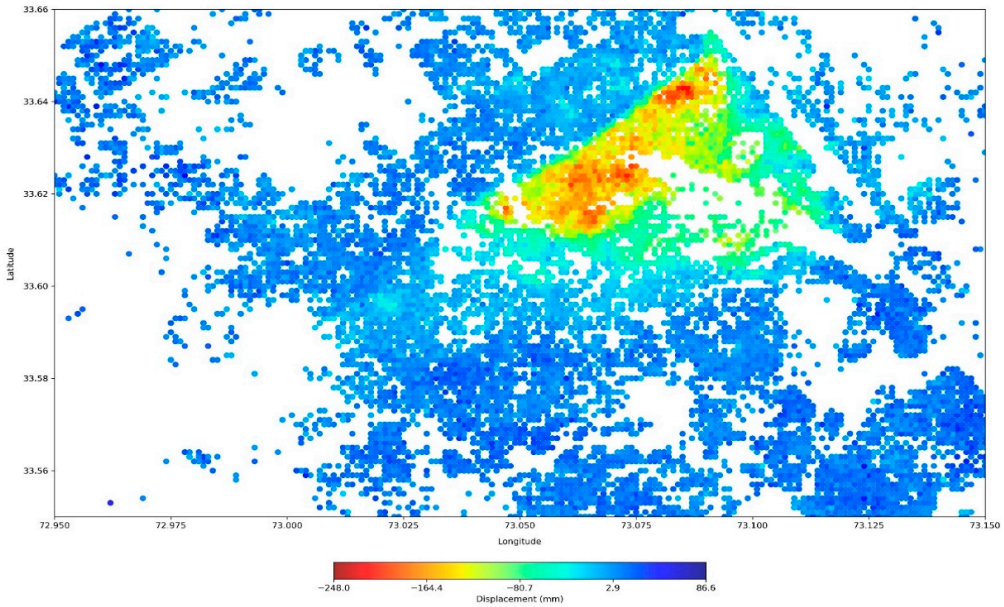

Figure 6. Vertical displacement was obtained by combining Sentinel-1 A ascending (6 December 2015 to 22 January 2023) path and descending path (31 March 2017 to 23 January 2023) utilizing non-linear PSInSAR.

Analysis of the vertical displacement map in Figure 6 reveals critical insights into the deformation patterns within the study area, situated between two uplift zones. This spatial arrangement underscores the significant influence of tectonic forces, challenging a prior study [24] that attributed the deformation solely to water extraction. A detailed examination of Figure 6 shows the deformation zone with a maximum subsidence of −248 mm, a clear marker of considerable ground surface lowering. This substantial subsidence suggests downward movement of the ground surface.

Moreover, the uplift zones to the north and south of the deformation area signal tectonic movements, manifesting as an upward thrust of the ground. The maximum uplift recorded is 86 mm. These findings emphasize the significant vertical displacement during the analyzed period, shedding light on the deformation dynamics and the potential involvement of tectonic forces. To gain a more comprehensive understanding of the role of tectonics, it is essential to analyze the deformation patterns along a tectonic map.

4.3. Factors Influencing Deformation

In the context of the seismic events and through the analysis of non-linear PSInSAR measurements, a multitude of factors emerges as pivotal to the observed deformation in

the study area. The interplay of tectonic setting, fault geometry, lithology [41], earthquake source characteristics, groundwater depletion [42], pore pressure alteration, geotechnical properties, and infrastructural or human activities delineates the complex framework influencing deformation. Understanding these mechanisms, particularly the interaction between tectonics, fault geometry, and lithological responses during seismic activities, is crucial.

Deformation Mapping and Geological Analysis

The deformed zones are located in the eastern part of the North Potwar deformed zone (NPDZ), which consists of complex folded and faulted structures. These structural elements exhibit a considerable parallel alignment, as shown in Figure 7. Key structural features of the area include the Soan syncline, Dhurnal blind thrust (DBT), and Khairi Murat thrust (KMT). These fault lines have been instrumental in sculpting the NPDZ's present tectonic landscape [36]. These faults are associated with seismic events, as indicated in Table 1. The earthquake record since 1875 shows ongoing seismicity in the region, with the most recent earthquake occurring in 2017 within the deformation zone, as illustrated in Figure 7. Additionally, three seismic events in 1977 with magnitudes of 4.6, 4.1, and 4.0, were observed on the eastern side of the blind faults that dissect the deformation zone, suggesting a potential influence on the observed deformation (Figure 8).

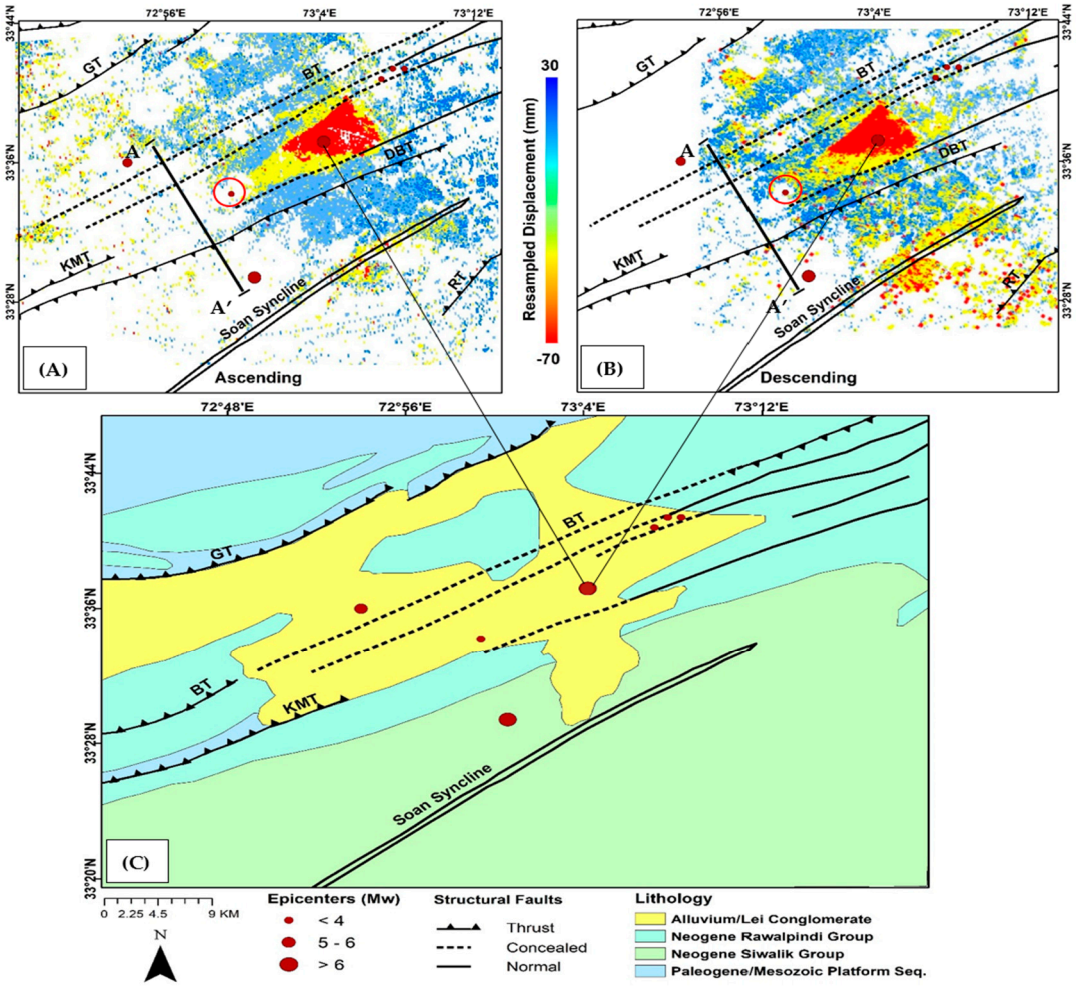

Figure 7. The resampled deformation displacement, structural fault lines, geology lines, geology, and recent earthquakes in the study area are shown. (**A**) Resampled deformation velocity of Sentinel-1 data along an ascending track. (**B**) Resampled deformation velocity of Sentinel-1 data along the descending track. The red circle along the epicenter shows the 2017 earthquake, whereas AA' is the cross-section shown in Figure 8. (**C**) Geological map of the study area displaying lithology and structural faults in the study area.

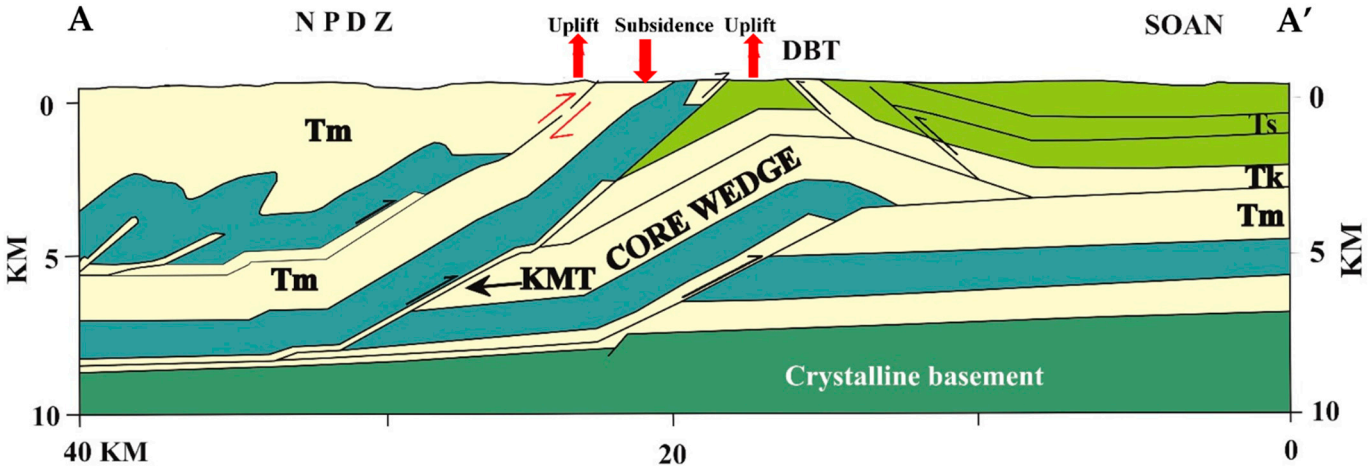

Figure 8. Modified from [32]; KMT = Khairi Murat thrust; NPDZ = North Potwar deformed zone; DBT = Dhurnal backthrust; Tm = Murree Fm; Tk = Kamlial Fm; Ts = Soan formation. The red arrows indicate the proposed deformation pattern in the study area.

The overlay of non-linear PSInSAR deformation results on the tectonic map (Figure 7) shows the presence of multiple faults traversing the study area. These faults encompass various types including thrust, reverse, and concealed faults. The deformation zone aligns with the blind fault in the region. After a more detailed analysis, numerous faults were observed near the deformation zone. Of particular significance were two faults that were blind or concealed in addition to the Bokra thrust (BT), which originates in the northern region of the deformation zone. In contrast, the Khairi Murat thrust (KMT) fault and Dhurnal back thrust (DBT) in the south exhibited the closest proximity to the deformation zone and were also in close vicinity to the epicenter of the 2017 earthquake, as shown by the red circle in Figure 7.

Meanwhile, lithological layers in the area encompass various rock formations such as alluvium/Lei conglomerate, Neogene Rawalpindi group, Neogene Siwalik group, and Paleogene/Mesozoic platform sequences. The integration of PSInSAR deformation results of the ascending and descending orbits with the tectonic geological map, as illustrated in Figure 7, has provided valuable insights regarding the sources of deformation within the study area. The analysis reveals that a blind fault possibly contributes to the deformation in the area, suggesting that it is likely to be one of the sources of the observed deformation in the deformation zone. In the northern region, the Bokra thrust (BT) fault exhibits uplift, whereas the Khairi Murat thrust (KMT) and Dhurnal back thrust (DBT) faults in the southern part also demonstrate uplift, with the deformation zone subsiding between these fault systems. The linear occurrence of deformation and these findings strongly indicate that fault activity is one of the contributing causes of the deformation observed in the study area, countering previous studies [24], which attributed it solely to water extraction.

Figure 7 illustrates uplift patterns along the DBT and KMT, capturing an upward shift in these regions, as tracked from ascending and descending data. While uplift rates are subtler compared to the −70 mm/year subsidence in the core deformation zone, they are crucial for understanding the area's tectonic dynamics. Uplift along the BT path in the north underscores the complex interactions between fault systems. The uplift observed in the northern region provides valuable information regarding the ongoing tectonic activity and highlights the potential role of these faults in the overall deformation process.

The epicenter of the 2017 earthquakes was located within the Lei conglomerates of recent deposits (Figure 7). These alluvial conglomerates comprise loose sediments such as gravel, sand, and silt. Subsidence in these sediments occurs through several mechanisms, including the rapid increase in pore water pressure induced by seismic waves. This phenomenon leads to a loss of shear strength and transforms sediments into a fluid-like state, resulting in liquefaction and subsequent sinking or subsidence. In addition, dynamic

compaction occurs as seismic waves exert cyclic loading and unloading forces, causing sediments to densify and compact, leading to subsidence. Vibrations generated during earthquakes can also induce settlement or consolidation of alluvium conglomerates, causing subsidence as the sediments settle under the influence of gravity. In some cases, geological faults produce fracturing within loose sediments, leading to differential subsidence, as depicted in Figure 7.

Figure 7 shows the significant deformation observed between the BT and DBT faults, primarily occurring in the alluvium/Lei conglomerate strata. Previous studies indicate that alluvial deposits such as the Lei conglomerate are susceptible to deformation owing to their granular nature and the mechanical properties of their constituent materials [43,44]. Although the increase in deformation due to earthquakes demonstrates the influence of lithology in the study area, as depicted in Figures 4 and 5, it is important to note that deformation patterns are not solely dictated by lithological variations. For instance, deformation diminishes in the vicinity of the DBT fault, despite the presence of alluvium/Lei conglomerates in that area. Furthermore, deformation abruptly ceases to the north along the concealed fault even within the same lithological context. Meanwhile, we observe uplift both to the north and south of the deformation zone, occurring in the alluvium/Lei conglomerates and the Neogene Rawalpindi group.

In brief, integrating PSInSAR findings into the tectonic map revealed the presence of multiple faults, including concealed faults, inside the designated research region. While the Khairi Murat thrust (KMT) fault in the south is close to the deformation zone and epicenter of the 2017 earthquake, it does not appear to be the primary cause of the observed deformation. Instead, the blind fault in the northern part of the deformation zone demonstrates a stronger association. The analysis also emphasizes uplift along the Bokra thrust (BT) fault in the north and the Dhurnal back thrust (DBT) and Khairi Murat thrust (KMT) faults in the south, indicating ongoing tectonic activity. These findings highlight the intricate nature of fault systems, their lithology, and their significant influence on deformation patterns within the study area.

5. Discussion

Our study leverages the non-linear PSInSAR approach to analyze deformation in the Islamabad/Rawalpindi region, indicating substantial tectonic activities. The non-linear aspect is critical for capturing these dynamics. By focusing on a specific window of 11 consecutive interferograms, we ensure a more precise analysis of the tectonic activities within the study area. This approach contrasts with prior research, which predominantly attributed deformation to anthropogenic factors, such as water extraction. For example, ref. [24] emphasized urban activities as the primary deformation driver, contrasting with our findings that underscore tectonic movements, especially after the 2017 earthquake. The non-linear methodology's strength lies in unveiling tectonic dynamics overlooked by traditional PSInSAR techniques. This methodological divergence possibly accounts for the differences in our conclusions compared with [24].

The current study utilizes non-linear PSInSAR techniques to evaluate this particular region, revealing a concealed yet dynamic, active geological structure. Our analysis situates the subsidence within the east–west-trending BT and KMT fault system, aligning with the observed deformation scale. This is consistent with the results reported in [45], where significant transformations within the NPDZ's eastern flank were reported, highlighting the area's complexity and ongoing seismic activity, as evidenced by several blind thrust faults where a frontal tip line is buried. Jaswal [31] marked these blind thrusts using seismic lines. Ref. [30] argued that this part of the Potwar Basin exhibited a strongly deformed, tapered fold and thrust belt. Geophysicists have determined that the faults are shifting from east–west to northeast in direction, concluding that these segments are seismically active and are involved with the basement in this complex deformation [37], as illustrated in Figure 8, a cross-section of these faults.

This cross-section spans 40 km, delving into the geology and tectonics up to a depth of 10 km. Several tectonic features can be seen between the NPDZ and the Soan syncline, including the Dhurnal back thrust (DBT) and Khairi Murat thrust (KMT), as shown in Figure 8. The indications surrounding these show uplift, with an upward direction indicating uplift and a downward tip indicating subsidence.

Figure 8 illustrates a geological structure characterized by a distinctive flat–ramp–flat shape within the core wedge positioned between the Dhurnal back thrust and the Khairi Murat thrust. The back thrusts display gradually increasing angles as the depth increases, ultimately converging at the tip of the blind-floor thrust. Notably, the flat region within the lower block of the core wedge remains unaffected within this specific segment, suggesting that the Dhurnal pop-up terminates towards the east. The core wedge undergoes approximately 4.5 km of horizontal compression, while the maximum displacement observed between the cutoff points measures approximately 5.5 km (Figure 8).

Our interpretations suggest the 2017 blind thrust initiation led to an uplift in the hanging wall block and subsidence in the footwall block (Figure 8). Interestingly, the non-linear PSInSAR analysis revealed that the blind thrust exhibited surface subsidence, aligning with the linear and parallel faulting previously identified by geologists [32]. These seismic activities also induced upward movement in the core wedge of the Khairi Murat thrust (KMT), leading to uplift (Figure 8). The increased deformation observed after the 2017 earthquake supports our conclusion that the subsidence is related to active blind thrusting along the KMT fault system, with a blind thrust located north of the Dhurnal blind thrust (DBT) and south of the Bokra thrust (BT), which is responsible for the recent subsiding activity in the study area. However, it is important to consider other factors such as groundwater depletion, water extraction, and other anthropogenic activities, in addition to the observed changes.

By integrating the non-linear PSInSAR deformation patterns with existing literature and tectonic models, we identified and analyzed surface changes linked to active tectonics and seismicity. This approach facilitates an improved understanding of the complex interplay between lithological, hydrological, and tectonic factors that shape the deformation patterns of the study area and landscape evolution.

Despite valuable insights, our study faces limitations, including the lack of pre-earthquake descending track Sentinel-1 data, which challenges our understanding of pre-2017 deformation patterns. Additionally, the anomalous deformation behavior observed in 2020 suggests the presence of complex factors influencing deformation, necessitating further investigation. Understanding the origins and implications of this anomaly is crucial, as it could reveal new aspects of tectonic behavior or other influencing factors.

Moreover, the PSInSAR technique, while widely used in urban areas, faces limitations when applied in non-urban regions. This is due to the scarcity of permanent scatterers in non-urban areas. This limitation restricts our ability to map deformation trends and analyze the impact of earthquakes in non-urban areas. Additionally, our interpretations and understanding of the various processes influencing deformation would benefit from incorporating additional data types. Data on subsurface characteristics, geotechnical properties, groundwater levels, and anthropogenic factors would provide a more comprehensive view of the forces at play and their relative contributions to the observed deformation patterns.

To address these challenges and enhance the scope of our research, we propose several approaches for future studies. Firstly, emphasis should be on continuous monitoring using available ascending and post-March 2017 descending track data, enabling a detailed analysis of ongoing deformation trends. Secondly, the implementation of other InSAR techniques, especially those that combine persistent and distributed scatterers like SqueeSAR, would significantly improve deformation mapping in urban and non-urban areas. These techniques would enable a more comprehensive understanding of surface displacements.

Moreover, future research should also focus on the 2020 anomaly. Investigating this anomaly will involve analyzing additional factors such as atmospheric dynamics, geological changes, and data-processing methods. A dedicated study on this anomaly could provide critical insights into its causes and effects, thereby enriching our understanding of the region's complex seismic and tectonic activities. Lastly, expanding the dataset to include information on subsurface characteristics, geotechnical properties, groundwater levels, and anthropogenic activities would greatly enhance the accuracy of our interpretations, leading to a deeper understanding of the complex dynamics influencing the region's deformation.

6. Conclusions

Permanent Scatterer Interferometry (PSInSAR) has proven to be a valuable tool for estimating the deformation in urban areas and monitoring short-term surface changes. Traditional PSInSAR, which treats surface deformation as a linear velocity, is well suited for short observation periods. Yet, for longer durations and capturing changes resulting from tectonic activity, such as the 2017 earthquake in our study area, non-linear PSInSAR stands out for its suitability. Overlaying the deformation map on the tectonic map revealed the encircling faults around the deformation zone, and the occurrence of the historical earthquake further underscores the role of tectonics in the study area. Non-linear PSInSAR adeptly pinpointed the deformation zone. This zone, located at the boundary of Islamabad/Rawalpindi, exhibited a deformation rate of up to 70 mm/year starting in December 2015.

Synthesizing non-linear PSInSAR, tectonic maps, vertical displacement decomposition (VDD), seismic records, and the literature suggests the deformation originates from a concealed fault. The deformation zone exhibited a downward dip, while the areas surrounding the north and south of the deformed region showed an uplift. This indicates a scenario in which the deformation zone is between two uplifting sections. Nevertheless, a critical limitation that surfaced during our investigation was the anomalous deformation behavior observed in 2020. While the cause of this anomaly remains elusive, future research endeavors will be dedicated to unraveling its origins, encompassing atmospheric dynamics, geological complexities, and potential data-processing artifacts.

Our findings emphasize the importance of advancing remote sensing methodologies to better understand complex geological processes. As we look ahead, we recognize the need for refined models capable of addressing the non-linear and heterogeneous nature of the deformation processes. Additionally, rigorous investigations into the causes and implications of the 2020 anomaly are essential to expand our knowledge in this field.

In conclusion, our study has showcased the capabilities of non-linear PSInSAR in detecting and monitoring tectonic-related changes within our study area. Although we have made significant strides in understanding the deformation patterns and their connection to tectonics, we acknowledge the pressing need for further research to unravel the remaining mysteries and refine our methodology.

Author Contributions: Conceptualization, Z.A. and T.B.; formal analysis, Z.A.; funding acquisition, T.B.; investigation, Z.A.; resources, T.B.; supervision, T.B.; visualization, Z.A. and A.A.; writing—original draft, Z.A.; writing—review and editing, Z.A., T.B., and A.A. All authors have read and agreed to the published version of the manuscript.

Funding: The APC was funded by the National Natural Science Foundation of China under Grant 42250610212.

Data Availability Statement: Sentinel-1 data are freely available from the Copernicus Data Space (https://dataspace.copernicus.eu, accessed on 3 February 2023).

Acknowledgments: We would like to thank Shuyi Yao for his significant contributions to the development of Equations (1) and (2) in the methodology section.

Conflicts of Interest: The authors declare no conflicts of interest.

References

1. Zhang, Y.; Liu, Y.; Jin, M.; Jing, Y.; Liu, Y.; Liu, Y.; Sun, W.; Wei, J.; Chen, Y. Monitoring Land Subsidence in Wuhan City (China) Using the SBAS-INSAR Method with Radarsat-2 Imagery Data. *Sensors* **2019**, *19*, 743. [CrossRef] [PubMed]
2. Zhang, Z.; Hu, C.; Wu, Z.; Zhang, Z.; Yang, S.; Yang, W. Monitoring and Analysis of Ground Subsidence in Shanghai Based on PS-InSAR and SBAS-InSAR Technologies. *Sci. Rep.* **2023**. [CrossRef] [PubMed]
3. Stanley, J.D.; Clemente, P.L. Clay Distributions, Grain Sizes, Sediment Thicknesses, and Compaction Rates to Interpret Subsidence in Egypt's Northern Nile Delta. *J. Coast. Res.* **2014**, *30*, 88–101. [CrossRef]
4. Cavalié, O.; Sladen, A.; Kelner, M. Detailed Quantification of Delta Subsidence, Compaction and Interaction with Man-Made Structures: The Case of the NCA Airport, France. *Nat. Hazards Earth Syst. Sci.* **2015**, *15*, 1973–1984. [CrossRef]
5. Hu, X.; Bürgmann, R.; Xu, X.; Fielding, E.; Liu, Z. Machine-Learning Characterization of Tectonic, Hydrological and Anthropogenic Sources of Active Ground Deformation in California. *J. Geophys. Res. Solid Earth* **2021**. [CrossRef]
6. Franzius, J.N.; Potts, D.M.; Addenbrooke, T.I.; Burland, J.B. The Influence of Building Weight on Tunnelling-Induced Ground and Building Deformation. *Soils Found.* **2004**. [CrossRef]
7. Milczarek, W.; Blachowski, J.; Grzempowski, P. Application of PSInSAR for Assessment of Surface Deformations in Post-Mining Area—Case Study of the Former Walbrzych Hard Coal Basin (SW Poland). *Acta Geodyn. Geomater.* **2017**. [CrossRef]
8. Khorrami, M.; Abrishami, S.; Maghsoudi, Y.; Alizadeh, B.; Perissin, D. Extreme Subsidence in a Populated City (Mashhad) Detected by PSInSAR Considering Groundwater Withdrawal and Geotechnical Properties. *Sci. Rep.* **2020**. [CrossRef]
9. Mohamadi, B.; Balz, T.; Younes, A. A Model for Complex Subsidence Causality Interpretation Based on PS-InSAR Cross-Heading Orbits Analysis. *Remote Sens.* **2019**, *11*, 2014. [CrossRef]
10. Khan, S.; Khan, M.A. Seismic Microzonation of Islamabad–Rawalpindi Metropolitan Area, Pakistan. *Pure Appl. Geophys.* **2018**, *175*, 149–164. [CrossRef]
11. Sheikh, I.M.; Pasha, M.K.; Williams, V.S.; Raza, S.Q.; Khan, K.S.A. Environmental Geology of the Islamabad-Rawalpindi Area, Northern Pakistan Regional Studies of the Potwar Plateau Area, Northern Pakistan. In *Regional Studies of the Potwar Plateau Area, Northern Pakistan*; U.S. Geological Survey: Baltimore, MD, USA, 2007.
12. Crosetto, M.; Monserrat, O.; Cuevas-González, M.; Devanthéry, N.; Crippa, B. Persistent Scatterer Interferometry: A Review. *ISPRS J. Photogramm. Remote Sens.* **2016**, *115*, 78–89. [CrossRef]
13. Yao, J.; Yao, X.; Liu, X. Landslide Detection and Mapping Based on SBAS-InSAR and PS-InSAR: A Case Study in Gongjue County, Tibet, China. *Remote Sens.* **2022**, *14*, 4728. [CrossRef]
14. Awasthi, S.; Jain, K.; Bhattacharjee, S.; Gupta, V.; Varade, D.; Singh, H.; Narayan, A.B.; Budillon, A. Analyzing Urbanization Induced Groundwater Stress and Land Deformation Using Time-Series Sentinel-1 Datasets Applying PSInSAR Approach. *Sci. Total Environ.* **2022**, *844*, 157103. [CrossRef] [PubMed]
15. Bakon, M.; Perissin, D.; Lazecky, M.; Papco, J. Infrastructure Non-linear Deformation Monitoring Via Satellite Radar Interferometry. *Procedia Technol.* **2014**, *16*, 294–300. [CrossRef]
16. Nahli, A.; Simonetto, E.; Tatin, M.; Durand, S.; Morel, L.; Lamour, V. On the Combination of PSINSAR and GNSS Techniques for Long-Term Bridge Monitoring. In Proceedings of the International Archives of the Photogrammetry, Remote Sensing and Spatial Information Sciences–ISPRS Archives, Nice, France, 31 August–2 September 2020.
17. Nahli, A.; Simonetto, E.; Merrien-Soukatchoff, V.; Durand, F.; Rangeard, D. Sentinel-1 for Monitoring Tunnel Excavations in Rennes, France. *Procedia Comput. Sci.* **2018**, *138*, 393–400. [CrossRef]
18. Ciampalini, A.; Bardi, F.; Bianchini, S.; Frodella, W.; del Ventisette, C.; Moretti, S.; Casagli, N. Analysis of Building Deformation in Landslide Area Using Multisensor PSInSARTM Technique. *Int. J. Appl. Earth Obs. Geoinf.* **2014**, *33*, 166–180. [CrossRef] [PubMed]
19. Ferretti, A.; Prati, C.; Rocca, F. Permanent Scatterers in SAR Interferometry. *IEEE Trans. Geosci. Remote Sens.* **2001**, *39*, 8–20. [CrossRef]
20. Hooper, A.; Segall, P.; Zebker, H. Persistent Scatterer Interferometric Synthetic Aperture Radar for Crustal Deformation Analysis, with Application to Volcán Alcedo, Galápagos. *J. Geophys. Res. Solid Earth* **2007**, *112*, B7. [CrossRef]
21. Berardino, P.; Fornaro, G.; Lanari, R.; Sansosti, E. A New Algorithm for Surface Deformation Monitoring Based on Small Baseline Differential SAR Interferograms. *IEEE Trans. Geosci. Remote Sens.* **2002**, *40*, 2375–2383. [CrossRef]
22. Ferretti, A.; Fumagalli, A.; Novali, F.; Prati, C.; Rocca, F.; Rucci, A. A New Algorithm for Processing Interferometric Data-Stacks: SqueeSAR. *Proc. IEEE Trans. Geosci. Remote Sens.* **2011**, *49*, 3460–3470. [CrossRef]
23. Jiang, H.; Balz, T.; Cigna, F.; Tapete, D. Land Subsidence in Wuhan Revealed Using a Non-linear PSInSAR Approach with Long Time Series of COSMO-SkyMed SAR Data. *Remote Sens.* **2021**, *13*, 1256. [CrossRef]
24. Khan, J.; Ren, X.; Hussain, M.A.; Jan, M.Q. Monitoring Land Subsidence Using PS-InSAR Technique in Rawalpindi and Islamabad, Pakistan. *Remote Sens.* **2022**, *14*, 3722. [CrossRef]
25. Samieie-Esfahany, S.; Hanssen, R.F.; van Thienen-visser, K.; Muntendam-bos, A.; Samiei-Esfahany, S.; Hanssen, R.F.; van Thienen-visser, K.; Muntendam-bos, A. On the Effect of Horizontal Deformation on InSAR Subsidence Estimates. In Proceedings of the Fringe 2009 Workshop, Frascati, Italy, 30 November–4 December 2009.
26. Gee, E.R.; Gee, D.G. *Overview of the Geology and Structure of the Salt Range, with Observations on Related Areas of Northern Pakistan*; Geological Society of America: Boulder, CO, USA, 1989. [CrossRef]
27. Auden, J.B.; Gansser, A. Geology of the Himalayas. *Geogr. J.* **1967**, *133*, 84. [CrossRef]

28. Treloar, P.J.; Coward, M.P.; Chambers, A.F.; Izatt, C.N.; Jackson, K.C. Thrust Geometries, Interferences and Rotations in the Northwest Himalaya. In *Thrust Tectonics*; Springer: Berlin/Heidelberg, Germany, 1992.
29. McDougall, J.W.; Hussain, A.; Yeats, R.S. The Main Boundary Thrust and Propagation of Deformation into the Foreland Fold-and-Thrust Belt in Northern Pakistan near the Indus River. *Geol. Soc. Spec. Publ.* **1993**, *74*, 581–588. [CrossRef]
30. Jaume, C.; Lillie, R.J. Mechanics of the Sal Trange Potwar Plateau, Pakistan: A Fold and Thrust Best Underlain by Evaporites. *Tectonics* **1988**, *7*, 57–71. [CrossRef]
31. Jadoon, I.A.K.; Frisch, W.; Kemal, A.; Jaswal, T.M. Thrust Geometries and Kinematics in the Himalayan Foreland (North Potwar Deformed Zone), North Pakistan. *Geol. Rundsch.* **1997**, *86*, 120–131.
32. Jadoon, I.A.K.; Frisch, W.; Jaswal, T.M.; Kemal, A. Triangle Zone in the Himalayan Foreland, North Pakistan. *Spec. Pap. Geol. Soc. Am.* **1999**, *328*, 275–286. [CrossRef]
33. Di Giacomo, D.; Robert Engdahl, E.; Storchak, D.A. The ISC-GEM Earthquake Catalogue (1904–2014): Status after the Extension Project. *Earth Syst. Sci. Data* **2018**, *10*, 1877–1899. [CrossRef]
34. Mehdi, S.K. Water and Power Development Authroity Simly Dam Project Seismotectonics & Seismic Hazard Analysis Volume-I September 2015 Submitted By Directorate of Seismic Studies Office of the General Manager & Project Director Tarbela Dam Project. *J. Artic.* **2015**, *I*, 1–58.
35. Riaz, M.; Pimentel, N.; Ghazi, S.; Zafar, T.; Alam, A.; Ariser, S. Lithostratigraphic Analysis of the Eocene Reservoir Units of Meyal Area, Potwar Basin, Pakistan. *Himal. Geol.* **2018**, *39*, 161–170.
36. Jaswal, T.M.; Lillie, R.J.; Lawrence, R.D. Structure and Evolution of the Northern Potwar Deformed Zone, Pakistan. *Am. Assoc. Pet. Geol. Bull.* **1997**, *81*, 308–328. [CrossRef]
37. Lisa, M.; Khan, S.A.; Khwaja, A.A. Focal Mechanism Study of North Potwar Deformed Zone, Pakistan. *Acta Seismol. Sin.* **2004**, *26*, 231–237. [CrossRef]
38. Pakistan Bureau of Statistics. *Pakistan Bureau of Statistics | 6th Population and Housing Census*; Pakistan Bureau of Statistics: Lahore, Pakistan, 2017.
39. Perissin, D.; Wang, Z.; Wang, T. The SARPROZ InSAR Tool for Urban Subsidence/Manmade Structure Stability Monitoring in China. In Proceedings of the 34th International Symposium on Remote Sensing of Environment–The GEOSS Era: Towards Operational Environmental Monitoring, Sydney, Australia, 10–15 April 2011.
40. Pepe, A.; Calò, F. A Review of Interferometric Synthetic Aperture RADAR (InSAR) Multi-Track Approaches for the Retrieval of Earth's Surface Displacements. *Appl. Sci.* **2017**, *7*, 1264. [CrossRef]
41. Bozzano, F.; Esposito, C.; Franchi, S.; Mazzanti, P.; Perissin, D.; Rocca, A.; Romano, E. Understanding the Subsidence Process of a Quaternary Plain by Combining Geological and Hydrogeological Modelling with Satellite InSAR Data: The Acque Albule Plain Case Study. *Remote Sens. Environ.* **2015**, *168*, 219–238. [CrossRef]
42. Figueroa-Miranda, S.; Tuxpan-Vargas, J.; Ramos-Leal, J.A.; Hernández-Madrigal, V.M.; Villaseñor-Reyes, C.I. Land Subsidence by Groundwater Over-Exploitation from Aquifers in Tectonic Valleys of Central Mexico: A Review. *Eng. Geol.* **2018**, *246*, 91–106. [CrossRef]
43. Zhao, G.; Guo, W.; Li, X. Mechanical Properties of Mega-Thick Alluvium and Their Influence on the Surface Subsidence. *Geotech. Geol. Eng.* **2020**, *38*, 137–149. [CrossRef]
44. Guo, W.; Zhao, G.; Bai, E.; Guo, M.; Wang, Y. Effect of Overburden Bending Deformation and Alluvium Mechanical Parameters on Surface Subsidence Due to Longwall Mining. *Bull. Eng. Geol. Environ.* **2021**, *80*, 2751–2764. [CrossRef]
45. Banks, C.J.; Warburton, J. "Passive-Roof" Duplex Geometry in the Frontal Structures of the Kirthar and Sulaiman Mountain Belts, Pakistan. *J. Struct. Geol.* **1986**, *8*, 229–237. [CrossRef]

Disclaimer/Publisher's Note: The statements, opinions and data contained in all publications are solely those of the individual author(s) and contributor(s) and not of MDPI and/or the editor(s). MDPI and/or the editor(s) disclaim responsibility for any injury to people or property resulting from any ideas, methods, instructions or products referred to in the content.